Electron Magnetic Resonance and Density Functional Theory Study of Room Temperature X-Irradiated β-D-Fructose Single Crystals

Mihaela Adeluta Tarpan,[†,§] Ewald Pauwels,[‡,||] Henk Vrielinck,[†] Michel Waroquier,[‡] and Freddy Callens*[,†]

Department of Solid State Sciences, Ghent University, Krijgslaan 281-S1, B-9000 Gent, Belgium, and Center for Molecular Modeling, Ghent University, Technologiepark 903, B-9052 Zwijnaarde, Belgium

Received: August 17, 2010; Revised Manuscript Received: October 20, 2010

Stable free radical formation in fructose single crystals X-irradiated at room temperature was investigated using Q-band electron paramagnetic resonance (EPR), electron nuclear double resonance (ENDOR), and ENDOR induced EPR (EIE) techniques. ENDOR angular variations in the three main crystallographic planes allowed an unambiguous determination of 12 proton HFC tensors. From the EIE studies, these hyperfine interactions were assigned to six different radical species, labeled F1−F6. Two of the radicals (F1 and F2) were studied previously by Vanhaelewyn et al. [Vanhaelewyn, G. C. A. M.; Pauwels, E.; Callens, F. J.; Waroquier, M.; Sagstuen, E.; Matthys, P. *J. Phys. Chem. A* **2006**, *110*, 2147.] and Tarpan et al. [Tarpan, M. A.; Vrielinck, H.; De Cooman, H.; Callens, F. J. *J. Phys. Chem. A* **2009**, *113*, 7994.]. The other four radicals are reported here for the first time and periodic density functional theory (DFT) calculations were used to aid their structural identification. For the radical F3 a C3 carbon centered radical with a carbonyl group at the C4 position is proposed. The close similarity in HFC tensors suggests that F4 and F5 originate from the same type of radical stabilized in two slightly different conformations. For these radicals a C2 carbon centered radical model with a carbonyl group situated at the C3 position is proposed. A rather exotic C2 centered radical model is proposed for F6.

Introduction

The study of free radicals induced by ionizing radiation in carbohydrates using electron magnetic resonance (EMR) techniques is interesting from many points of view. First, as carbohydrates are extremely abundant in plants and animals, they can be used as probes in detecting radiation exposure of sugar-containing foodstuffs.[1,2] Furthermore, electron paramagnetic resonance (EPR) and related techniques can be used to understand the identity and the structural properties of the involved radicals. A number of studies are available that focus on the identification of the radiation-induced radicals in single crystals of various carbohydrates, such as glucose,[3,4] sucrose,[5−9] sorbose,[10] or rhamnose.[11−15]

A clear insight in the radiation chemistry of sugar radicals is very important for understanding the radiation damage processes of more complex systems, like DNA.[16] Sugar radicals play an important role in the irradiation process of DNA, because they almost invariably lead to strand breaks and when produced on both strands in proximity of each other they can result in a lethal double strand break.

The structural identification of the free radicals obtained after X-irradiation in this type of organic materials is in most cases the result of a combination of magnetic resonance experiments (EPR and/or electron nuclear double resonance (ENDOR)) and theoretical calculations, often based on density functional theory (DFT). These ab initio methods allow the optimization of a tentative radical structure and the calculation of spin Hamiltonian parameters. By then comparing calculated and measured parameters, primarily proton hyperfine coupling tensors (HFC tensors), the validity of a proposed radical model can be assessed.

One of the carbohydrates that has attracted considerable attention in the past decade is β-D-fructose. The radiation chemistry of this "simple" sugar in the solid state proves to be particularly complex, with different radicals dominating the EPR spectra depending on the irradiation and measurement temperature (see below).

The primary radicals or species closely related to the primary radicals in 10 K X-irradiated fructose single crystals were studied previously by Tarpan et al.[17]ENDOR angular variations in the three principal crystallographic planes and a fourth skewed plane allowed the unambiguous determination of five proton HFC tensors. From an extensive ENDOR-induced EPR (EIE) study these hyperfine interactions could be assigned to three different radicals, labeled T1, T1*, and T2. For the T1 and T1* radicals, the similarity in HFC tensors suggested that the same type of radical is formed in two slightly different conformations. DFT calculations identified their structure as being a C3 centered radical, formed by a net (H3) hydrogen abstraction (see Figure 1 for atom numbering). The T2 radical was identified as a C5 centered radical, again formed by a net hydrogen abstraction (H5). For both radicals, very good agreement between calculated and experimental HFC tensors was found.

Vanhaelewyn et al.[18] presented a detailed EPR/ENDOR and DFT study of β-D-fructose single crystals that were in situ X-irradiated at 80 K. The measurements revealed the presence of at least four carbon centered radicals. Two of them, labeled R1 and R1′, exhibit very similar proton HFCs (β-type), whereas

* To whom correspondence should be addressed. Tel: +32 9 264 43 52. Fax: +32 9 264 49 96. E-mail: Freddy.Callens@ugent.be.
† Department of Solid State Sciences.
‡ Center for Molecular Modeling.
§ Research assistant of the Fund for Scientific Research, Flanders (Belgium) (FWO - Vlaanderen).
|| Postdoctoral Fellow of the Fund for Scientific Research, Flanders (Belgium) (FWO - Vlaanderen).

10.1021/jp107777v
Published on Web 11/04/2010

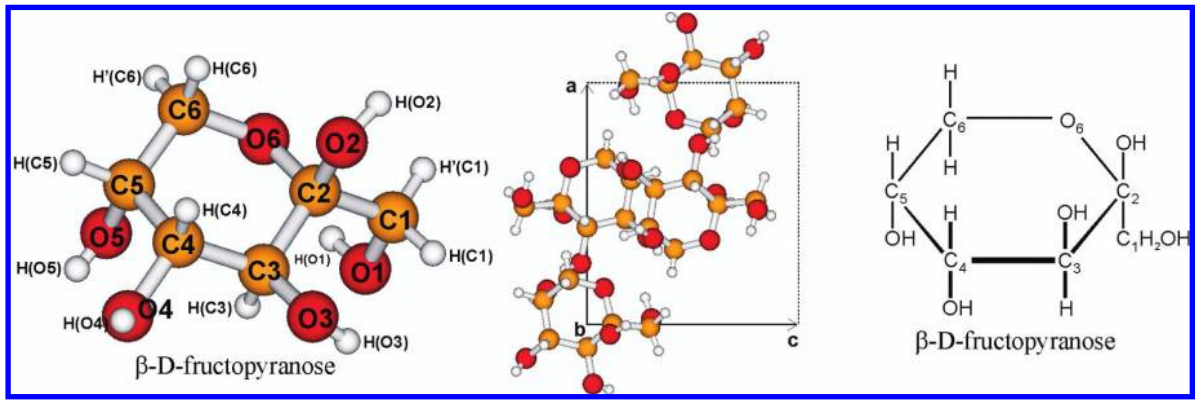

Figure 1. Left: molecular structure of β-D-fructose with labeled atoms. Central: four β-D-fructose molecules in the unit cell. Right: fructose chemical structure.

the other two radicals, R2 and R3, are also similar but are mainly characterized by an α-type coupling. For R1/R1′, a radical model obtained by abstraction of a hydrogen from C3 was proposed. The other radicals R2/R3 were suggested to be open ring species with a disrupted C2−C3 and a double C2−O2 bond. A possible formation mechanism for the open-ring species, starting from an alkoxy radical with the unpaired spin located on the O2 oxygen atom, was also presented.

The stable radicals in β-D-fructose single crystals, generated by room temperature (RT) X-irradiation, were investigated by Vanhaelewyn et al.[19] in a previous EPR/ENDOR study. To determine the number of components contributing to the experimental spectra, MLCFA (maximum likelihood common factor analysis) was used. Whereas the MLCFA analysis revealed at least four different components, ENDOR and EIE experiments allowed the determination of the proton HFC tensors for only two radicals, labeled F1 and F2. Weaker lines in the ENDOR spectra remained unassigned. The two stable radicals F1 and F2 are characterized by three proton HFCs. Again, the similarity of the HFC tensors for these radicals indicated that probably the same type of radical occurs in two slightly different conformations. A tentative structure for F1/F2 was proposed on the basis of DFT calculations: a C2-centered structure, resulting from hydroxyl abstraction.[19,20] However, in these studies the solid-state molecular environment of the radical was not at all taken into account in the DFT calculations. Also, the HFC tensor principal directions were either not analyzed[19] or only considered in a relative fashion.[20] Yet, later works by these authors[21] illustrated that incorporation of the molecular environment in these calculations can drastically alter the predicted pattern of HFC tensors. Furthermore, a good reproduction of the hyperfine tensor principal axes was found to be a very sensitive probe for the validity of a particular radical model structure. In that respect, the validity of the tentative F1/F2 radical structure is questionable.

In a later study,[22] the g-tensors of the F1 and F2 radicals were determined from angular dependent ENDOR-induced EPR (EIE) experiments. The relatively large anisotropy of these tensors suggested that F1/F2 are carbon-centered radicals but that the unpaired electron is considerably delocalized, e.g., onto a neighboring oxygen atom or carbonyl group. Furthermore, EPR measurements were performed on fructose powders, selectively ^{13}C enriched at different ring positions, with the primary aim of determining on which carbon atom the unpaired electron density is mainly localized. The powder EPR measurements suggested the C3 position as the center of unpaired electron density, further questioning the validity of the earlier tentative structural model.

In view of the discrepancy between their MLCFA and EMR results, Vanhaelewyn et al.[19] further suggested that the F1 and F2 radicals dominate the EPR spectrum. To check this hypothesis, they tried to reconstruct the experimental EPR spectra for the magnetic field along the crystallographic *a*, *b*, and *c* axes, using the proton HFC tensors obtained from the ENDOR angular variations and an isotropic *g* value. For the *b* axis a good agreement was found between the experimental and the corresponding simulated spectrum using only the two dominant components. For the *c* axis and other orientations the agreement was still fair but it was very clear that additional components are present.

These additional radicals are the main focus of the present study. Here, the results of careful EPR, ENDOR, and EIE experiments are presented for four additional radicals. The interpretation of the experimental data is supported by DFT calculations relying on a periodic scheme. In recent studies, this approach has proven particularly successful for the identification of several radiation-induced radicals in fructose,[17] sucrose,[8,9] rhamnose,[23] glucose-phosphate,[24,25] and even solid-state alanine.[26] Application of this methodology yields several plausible radical models for the less dominant radicals in RT-irradiated fructose, along with a few more tentative proposals.

Materials and Methods

Single crystals of β-D-fructose (Sigma-Aldrich) were grown from saturated aqueous solutions containing ethanol by slow evaporation at 40 °C. β-D-Fructose crystals are orthorhombic with space group symmetry $P2_12_12_1$ and four molecules in the unit cell (Figure 1).[27,28] The crystal axes were labeled according to a neutron diffraction study,[27] i.e., $a = 0.9191$ nm, $b = 1.0046$ nm, and $c = 0.8095$ nm. *a*, *b*, and *c* were chosen as the reference axes for EMR experiments. In Figure 1 the molecular structure of β-D-fructose together with the four β-D-fructose molecules at four different crystallographic sites, is shown.

For the identification of the crystal axes, single crystals of β-D-fructose were mounted onto a goniometer head of a Weissenberg X-ray diffraction camera. Using oscillation diagrams, the rotation axis was aligned within 1° along one of the crystal axes to be used as the crystal rotation axis in the EPR/ENDOR experiment. The crystals were then transferred and glued to quartz crystal holders without loss of alignment.

The single crystals were X-irradiated at RT with a dose of approximately 30 kGy using a Philips tungsten anticathode X-ray tube operated at 60 kV and 40 mA.

The Q-band spectra were recorded using a Bruker Elexsys E500 Q-band spectrometer equipped with an Oxford CF935

cryostat and a maximum available microwave power of 160 mW. The magnetic field and the microwave frequency were measured using a Bruker ER035 M NMR Gaussmeter and an EIP 548B microwave frequency counter.

The EPR and ENDOR measurements were performed in the three principal crystallographic planes (*ab*, *ac*, and *bc* planes) by rotating the sample in 5° steps over 100°. The EIE measurements were performed with the magnetic field along the crystallographic axes and helped to assign the various ENDOR lines to particular radicals. To determine the proton HFC tensors from the ENDOR angular variations, the MAGRES[29] program was used. For simulations of EPR and EIE spectra and the ENDOR angular variations the EasySpin[30] routines in Matlab were used. During the extraction of the principal values and directions of the HFC tensors from ENDOR significant attention was paid to the Schonland ambiguity.[31,32]

Computational Details

All DFT calculations were performed in a periodic approach, using the CP2K software[33] and the BLYP functional.[34,35] The crystallographic unit cell of fructose[27] was chosen as the basic unit for the periodic boundary conditions. The Gaussian and plane waves (GPW) dual basis set method[36] was used in all geometry optimizations, employing a TZVP triple-ζ Gaussian basis set[37] and plane waves (400 Ry density cutoff) with GTH pseudopotentials.[38,39] For the subsequent **g** and HFC tensor calculations, we relied on recent implementations[40,41] in the CP2K code, employing the all-electron Gaussian and augmented plane wave (GAPW) method.[42] The density cutoff for the auxiliary plane wave basis set was again 400 Ry, and the all-electron TZVP basis[43] was used.

Radical models were obtained by modifying the structure of the crystallographic unit cell and by subsequently optimizing this initial geometry. A large amount of modifications was attempted, on the basis of the typical radiation-induced reactions commonly observed in sugar systems: hydrogen atom abstraction/addition from/to carbon or oxygen, hydroxy group abstraction, rupture of the sugar ring backbone, β elimination, 1,2- and 1,4-hydrogen shifts, net H_2 abstraction, and combinations thereof, generating a list of 60 model structures (taken up in the Supporting Information). Although this list does not exhaustively comprise all possible combinations of these modifications, they represent the most obvious choices based on (chemical) intuition and an initial screening of the experimental hyperfine principal directions (see later). Some of the models were based on the suggestions made in refs 44 and 45. A complete examination of all conformational degrees of freedom of any radical model is beyond the scope of this work. And so, in principle, it cannot be ruled out that a particular radical model assumes a specific conformation that incidentally does yield a good agreement with the experimental data. Yet, this possibility seems remote on the basis of a (limited) conformational analysis performed for one of the radical models (M11). Although alternative minima were found, these always proved to be local with far less favorable energies than the global minimum (which is reported in this work). In addition, the simulated EPR properties for these local minima were always found to still resemble those of the global minimum. Certainly none of these alternate minima would have led to different conclusions.

Results

EPR, ENDOR, and EIE of β-D-Fructose Single Crystals. All EPR, ENDOR, and EIE measurements were carried out at 55 K. In Figure 2, typical EPR and EIE Q-band spectra obtained after RT X-irradiation, with the magnetic field along the *a* axis are shown. A typical EPR spectrum consists of many strongly overlapping broad resonance lines around $g = g_e$.

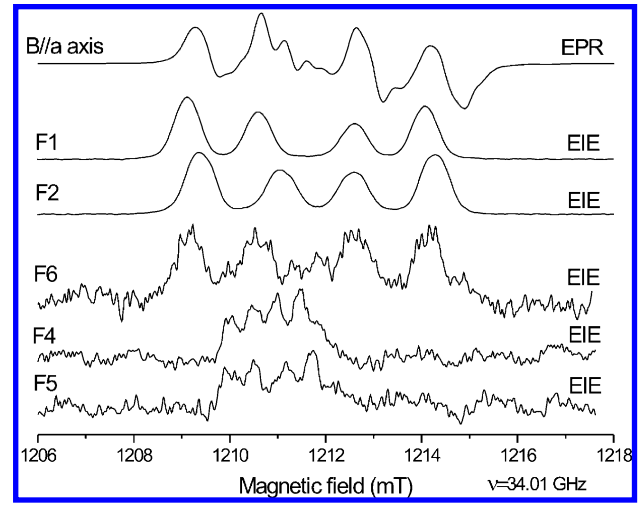

Figure 2. Q-band EPR and EIE spectra recorded at 55 K of β-D-fructose single crystals X-irradiated at RT for the magnetic field parallel to the *a* axis.

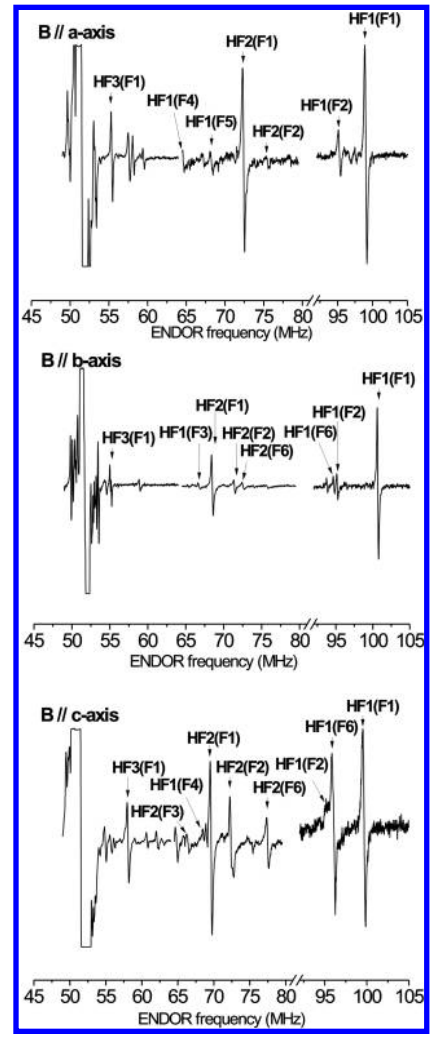

Figure 3. Q-band ENDOR spectra from fructose single crystals X-irradiated at RT for the magnetic field along the three crystallographic axes.

Twelve HFC tensors could be determined from ENDOR angular variations in the three principal crystallographic planes.

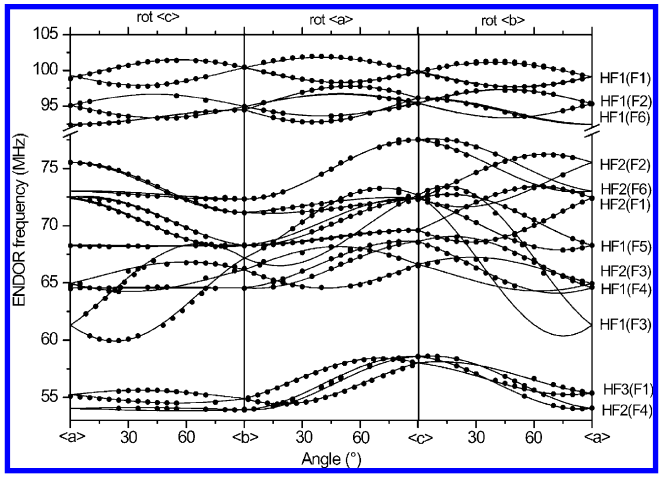

Figure 4. ENDOR angular variation in all three principal planes. The solid circles represent the experimental points for the 12 interactions for which proton HFC tensors were determined, and the solid lines through the circles are the simulations using the data in Tables 1 and 2.

In Figure 3, typical ENDOR spectra for the magnetic field along the principal crystallographic axes are shown. For each orientation, the ENDOR spectra were recorded at a couple of different magnetic field values in the EPR spectra, to determine all the relevant resonance lines. In Figure 3, only the ENDOR spectra with most of the interactions present are shown. In Figure 4 the angular dependence of all assigned ENDOR lines is shown.

Five of these HFC tensors, labeled HF1(F1), HF2(F1), HF3(F1), HF1(F2), and HF2(F2), closely resemble those that were already reported by Vanhaelewyn et al.[19] in a previous EPR/ENDOR study on β-D-fructose single crystals X-irradiated at RT. The EIE measurements in the present work, confirm that these five proton HFC interactions can be assigned to two different radicals (F1 and F2), which are the dominant contributions to the EPR spectra (Figure 2). Each of the F1 and F2 radicals exhibits three β proton HFCs: a large coupling around 100 MHz, an intermediate coupling around 40 MHz, and a relatively small coupling around 10 MHz (Table 1). Although for the F1 radical all three HFC tensors could be determined from the ENDOR angular variations, it proved impossible to resolve the small interaction for F2. The ENDOR lines could not be followed in a sufficient number of planes to allow an accurate determination of the corresponding tensor.

The main focus of the present work is the study of the other seven HFC tensors, labeled HF1(F3), HF2(F3), HF1(F4), HF2(F4), HF1(F5), HF1(F6), and HF2(F6), which have not been reported in the literature before (Table 2). Since their contributions to the EPR spectrum are less dominant than those from F1 and F2, their characterization was particularly challenging, and to distinguish between the dominant and the nondominant radicals, ENDOR measurements had to be performed with the magnetic field locked at different positions in the EPR spectra.

EIE experiments showed that these couplings could be ascribed to four different radicals. The radical F3 is characterized by two hyperfine interactions: one α-type HFC with an isotropic value of around -31 MHz (HF1(F3)) and a β-type HFC close to 29 MHz (HF2(F3)). A complete angular variation of two very similar β-type couplings (HF1(F4) and HF1(F5)) was obtained in the three principal planes. These couplings were assigned to two different radicals labeled F4 and F5. The similarity of the HFC tensors HF1(F4) and HF1(F5) suggests that they originate from the same type of radical in two slightly different conformations, as often occurs in these kind of crystals.[7,17,18] For the radical F4, one of the smaller hyperfine interactions could be followed in all three principal planes and so a tensor could be determined for it (HF2(F4)). It is either a β-type or γ-type hyperfine interaction with an isotropic value of about 8 MHz. Finally, the radical denoted F6 exhibits two very clear β-type proton HFCs: one large coupling (HF1(F6)) around 86 MHz and a second smaller coupling (HF2(F6)) close to 46 MHz. Although the EIE spectra corresponding to the F6 radical are very similar to the EIE spectra of the F1/F2 radical, the substantial difference in principal directions suggest that they originate from a completely different type of radical.

We carefully investigated the influence of the four additional radicals (F3−F6) on the experimental EPR spectra and for the $\langle a \rangle$ direction in particular, which is the most sensitive in this respect. In Figure 5a,b and in the studies of Vanhaelewyn et al.[19] and Tarpan et al.[22] it is demonstrated that a simulation using only F1 and F2 can account for the major part of the EPR spectra.

Quantifying the contribution of the six radicals is quite complicated and not completely unambiguous, certainly for the weaker components F3−F6. This is mainly due to the incomplete knowledge of some HFCs, line width parameters, the **g**-tensor of F3 (absence of the EIE spectrum) and the similarity of the F6 and the F1/F2 spectra.

TABLE 1: Experimental Proton HF Tensors (MHz) for the F1 and F2 Radicals in Fructose Single Crystals X-Irradiated at RT, Obtained from Q-Band ENDOR Measurements at 55 K[a]

					principal directions		
radical	tensor	principal values	anisotropic values	isotropic value	*a*	*b*	*c*
F1	HF1(F1)	103.54(2)	7.08(2)	96.46(2)	0.504(1)	0.647(9)	0.572(3)
		93.64(2)	−2.82(2)		0.179(1)	−0.726(1)	0.664(8)
		92.19(2)	−4.26(2)		0.845(1)	−0.232(6)	−0.482(6)
	HF2(F1)	43.99(2)	6.78(2)	37.21(3)	0.887(1)	−0.097(4)	0.452(5)
		34.41(3)	−2.79(3)		0.363(2)	−0.460(14)	−0.811(7)
		33.22(3)	−3.99(3)		0.287(1)	0.883(6)	−0.372(13)
	HF3(F1)	14.03(3)	4.85(2)	9.19(2)	−0.140(5)	0.315(2)	−0.939(4)
		8.02(2)	−1.17(2)		0.912(2)	0.409(5)	0.002(3)
		5.51(2)	−3.68(2)		0.385(1)	−0.856(4)	−0.344(2)
F2	HF1(F2)	94.33(3)	6.97(3)	87.36(3)	0.612(1)	0.517(12)	0.599(2)
		84.23(3)	−3.13(3)		−0.066(2)	−0.721(14)	0.690(3)
		83.52(3)	−3.84(3)		0.788(1)	−0.461(13)	−0.407(2)
	HF2(F2)	49.55(3)	6.50(3)	43.05(3)	0.915(1)	0.038(2)	0.401(7)
		40.49(3)	−2.56(3)		0.385(3)	−0.375(15)	−0.843(6)
		39.12(3)	−3.93(3)		0.119(1)	0.926(6)	−0.358(14)

[a] The numbers in parentheses represent the uncertainty in the last significant digit(s).

TABLE 2: Experimental Proton HF Tensors (MHz) for the F3, F4, F5, and F6 Radicals in Fructose Single Crystals X-Irradiated at RT, Obtained from Q-Band ENDOR Measurements at 55 K[a]

					principal directions		
radical	tensor	principal values	anisotropic values	isotropic value	*a*	*b*	*c*
F3	HF1(F3)	45.88(3)	−14.98(3)	−30.90(2)	0.296(3)	−0.357(11)	0.886(7)
		30.87(3)	0.03(3)		0.224(7)	0.876(14)	0.427(5)
		15.95(4)	14.95(3)		0.929(8)	−0.324(4)	−0.179(6)
	HF2(F3)	34.73(6)	5.94(6)	28.79(6)	0.386(6)	0.612(12)	−0.690(18)
		26.13(6)	−2.65(5)		−0.138(5)	0.701(5)	0.700(9)
		25.50(7)	−3.29(6)		0.912(7)	−0.366(12)	0.186(7)
F4	HF1(F4)	35.25(4)	6.38(4)	28.87(4)	0.303(8)	0.091(5)	−0.949(7)
		26.17(4)	−2.70(4)		0.230(7)	−0.973(4)	−0.019(12)
		25.18(2)	−3.69(2)		0.925(11)	0.213(9)	0.316(9)
	HF2(F4)	14.31(3)	6.26(3)	8.06(3)	−0.104(7)	−0.025(4)	0.994(19)
		5.14(3)	−2.91(3)		−0.823(6)	−0.564(6)	−0.072(5)
		4.71(3)	−3.34(3)		−0.558(13)	0.826(11)	−0.079(5)
F5	HF1(F5)	42.58(3)	6.25(3)	36.33(3)	0.280(12)	−0.063(7)	0.958(25)
		33.60(2)	−2.73(3)		0.051(15)	0.997(17)	0.051(2)
		32.81(3)	−3.52(3)		0.959(6)	−0.034(15)	−0.282(8)
F6	HF1(F6)	92.54(3)	6.90(3)	85.64(3)	0.014(2)	−0.578(5)	−0.816(7)
		82.54(3)	−3.10(3)		0.200(1)	0.801(15)	−0.564(4)
		81.84(4)	−3.80(3)		0.980(13)	−0.156(7)	0.127(4)
	HF2(F6)	52.21(3)	6.61(3)	45.60(4)	0.131(3)	−0.002(3)	0.991(7)
		42.95(5)	−2.65(4)		0.982(4)	−0.139(14)	−0.130(9)
		41.64(3)	−3.95(3)		0.138(5)	0.990(3)	−0.016(7)

[a] The numbers in parentheses represent the uncertainty in the last significant digit(s).

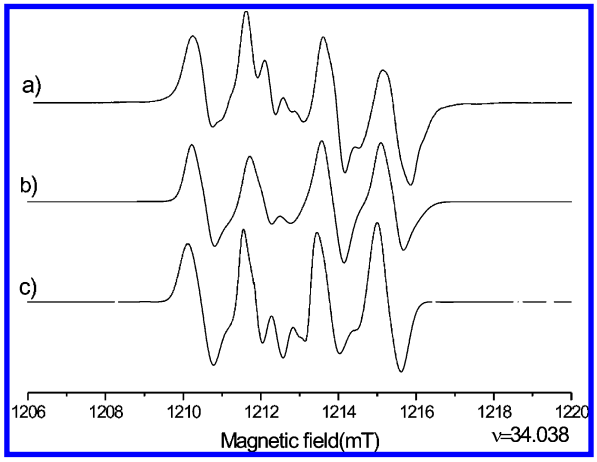

Figure 5. Experimental (a) and simulated Q-band EPR spectra for the magnetic field along the *a* axis for the case when only the contributions from the F1 (50%) and F2 (50%) radicals are considered (b) and when all six radicals are considered (c). The contributions from all six radicals are 30% F1, 30% F2, 10% F3, 5% F4, 5% F5, and 10% F6. For the simulations the hyperfine coupling tensors reported in Tables 1 and 2 and the **g** tensors reported by Tarpan et al.[22] for F1 and F2 were used. For the F4−F6 radicals the **g** value was determined from the EIE spectra and for F3 radical the free electron g value was used.

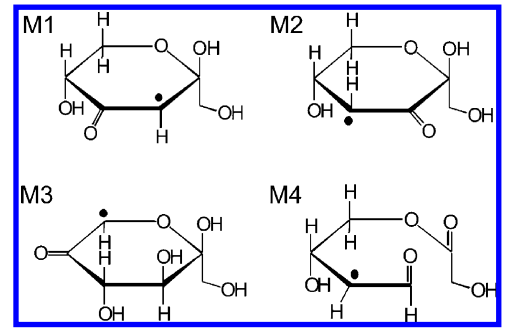

Figure 6. Chemical structures of the different models for radical F3 for which DFT calculations were performed (see Table 3).

A typical example of the improvement in spectrum reproduction that can be reached by introducing the extra components is shown in Figure 5c (simulation parameters, see caption). Several experimental features that cannot be explained by F1/F2 contributions are fairly well reproduced by adding the F3−F6 components. The relative importance of these four additional components can be estimated to be maximally 10% for either of them.

Radical Model Assignment. The main goal of studying radicals in sugar crystals with EPR and ENDOR is to obtain structural models for the radiation-induced radicals. Our previous experimental and computational work on the RT stable radicals in fructose has, however, demonstrated that finding suitable models is not at all trivial.

To obtain plausible radical models that may explain the observed resonances, the principal directions of the experimental HFC tensors were initially compared with the parameters derived from the pristine molecular structure. Because most of the HFCs determined in the present study are β-type interactions, the Heller−McConnell relation for the isotropic contribution was also used:[46,47]

$$a_{\mathrm{iso}}^{\beta} = \rho^{\pi}(B_0 + B_2 \cos^2 \theta) \qquad (1)$$

where θ is the dihedral angle between the $2p_z$ axis of the lone-electron orbital (LEO) on C_α and the $C_\beta-H_\beta$ bond, viewed along the $C_\alpha-C_\beta$ bond, ρ^π is the spin density in the LEO, and B_0 and B_2 are empirical constants, for which values of 0 and 126 MHz can be assumed in the present case.[47] The Heller−McConnell relation can then yield closer insight in the possible conformations of the radical (via the angle θ). This information considerably limits the number of possible radical models to be examined with the aid of DFT calculations.

Radical F3. This radical exhibits two appreciable HFCs. One of the couplings is due to an α-type proton hyperfine interaction, considering the characteristic symmetry of the anisotropic components ($+b_{\mathrm{aniso}}$, 0, $-b_{\mathrm{aniso}}$). However, both isotropic and anisotropic coupling values are substantially reduced compared

TABLE 3: Proton HFC Tensors (MHz) for Radical Models M1−M4 (Figure 5), Obtained by Means of DFT Calculations

				principal directions			
radical model	proton	isotropic values	anisotropic values	*a*	*b*	*c*	δ (deg)[a]
M1	H3	−38.18	−23.76	0.280	−0.437	0.855	5
			−3.89	0.347	0.876	0.335	9
			27.89	0.895	−0.203	−0.397	14
	H(O2)	17.71	5.53	0.372	0.647	−0.666	3
			−2.37	−0.160	0.752	0.640	5
			−3.28	0.914	−0.131	0.383	18
M2	H4	−37.17	−23.45	0.782	−0.039	0.622	37
			−3.51	0.134	0.985	−0.107	32
			27.19	0.609	−0.167	−0.776	41
	H6′	7.91	3.37	0.984	0.154	−0.092	58
			−1.26	−0.179	0.807	−0.563	79
			−2.09	0.013	−0.570	−0.822	86
	H(O5)	−6.76	−9.90	−0.265	−0.729	−0.631	
			0.10	−0.964	0.180	0.198	
			10.92	0.031	−0.660	0.750	
M3	H6	−32.06	−19.18	0.071	0.257	0.964	38
			−3.48	0.008	0.966	−0.258	42
			22.66	0.997	−0.026	−0.066	19
	H4	8.47	4.01	0.924	0.342	−0.173	47
			−1.44	0.029	0.388	0.921	24
			−2.57	0.382	−0.856	0.349	43
M4	H4	−36.38	−24.03	0.906	0.215	0.364	59
			−3.57	0.113	0.706	−0.699	70
			27.60	0.407	−0.675	−0.615	45
	H5	44.49	6.94	0.859	0.110	−0.500	42
			−3.25	0.512	−0.178	0.841	67
			−3.70	0.004	−0.978	−0.209	71

[a] δ (deg) are the angles between the principal directions of the experimental tensors for the F3 and the calculated tensors.

TABLE 4: Comparison of the C−H Directions in the Pristine Molecule with the Directions of the Eigenvectors Corresponding to the Most Positive Anisotropic Hyperfine Coupling Values of HF1(F4), HF2(F4), and HF1(F5)

		direction cosines			δ (deg)[a]		
	hydrogen position	*a*	*b*	*c*	HF1(F4)	HF2(F4)	HF1(F5)
C2−HC1	β	0.489	0.211	0.846	**14**	26	**16**
C2−H′C1	β	−0.209	0.223	0.978	**12**	**2**	**12**
C2−HC3	β	−0.325	−0.844	0.427	55	119	56
C2−HC4	γ	−0.286	0.154	0.946	**3**	**13**	**5**
C2−HC6	γ	0.594	0.442	0.673	31	42	33
C2−H′C6	γ	0.828	0.007	0.561	38	50	40
C3−HC4	β	0.054	0.592	0.804	34	35	35
C3−HC5	γ	0.622	0.122	0.774	21	33	23
C4−HC3	β	0.047	0.647	0.761	37	39	38
C4−HC5	β	0.835	0.032	0.550	39	51	40
C4−HC6	γ	0.779	0.583	−0.232	59	71	62
C4−H′C6	γ	0.970	0.141	−0.200	60	72	62
C5−HC4	β	0.855	−0.519	0.019	71	83	73
C5−HC6	β	0.313	0.853	−0.418	55	62	57
C5−H′C6	β	0.839	0.317	−0.443	45	58	47
C5−HC3	γ	0.603	0.430	0.672	31	42	33

[a] δ (deg) are the angles between the principal directions of the experimental and the calculated directions.

to those for a typical α-type proton HFC, indicating strong delocalization of the unpaired electron. The second interaction has an isotropic HFC of around 28 MHz and could originate from either a β-type or γ-type proton.

The spin density, for the case when an α-type proton is present, can be estimated using either the isotropic (McConnell relation,[47] eq 2) or the anisotropic values (Gordy−Bernhard[48] relation, eq 3)

$$a^{\alpha}_{\mathrm{iso}} = Q^{\alpha}_{\mathrm{iso}}\rho^{\pi} \tag{2}$$

$$b^{\alpha}_{+,\mathrm{aniso}} = Q^{\alpha}_{\mathrm{aniso}}\rho^{\pi} \tag{3}$$

where $a^{\alpha}_{\mathrm{iso}}$ is the isotropic component, $b^{\alpha}_{+,\mathrm{aniso}}$ is the most positive anisotropic component, ρ^{π} is the spin density in the $2p_z$ LEO of C_α, and $Q^{\alpha}_{\mathrm{iso}}$ and $Q^{\alpha}_{\mathrm{aniso}}$ are empirical values, dependent to some extent on the nature of the radical fragment. For $Q^{\alpha}_{\mathrm{iso}}$ a value of −72 MHz is generally assumed[49] and for $Q^{\alpha}_{\mathrm{aniso}}$ a value of 38.7 MHz was proposed.[50] Both equations yield unpaired spin densities of 0.40−0.45 for the F3 radical, indicating that more than 55% of the spin density is not localized on the C_α atom. Such a delocalization can occur when, for instance, the C_α

radical center is located next to a carbonyl group. In that case, the spin density will largely delocalize onto this π-system.

Reviewing all the radical models (see Supporting Information), only a few fit the general requirement of one α-type coupling, alongside one moderate HFC of β- or γ-type. The calculated hyperfine tensors for these models are given in Table 3, the corresponding model structures are shown in Figure 6. In all cases, the C_α radical center is adjacent to a carbonyl group.

Models M2 and M4 can be readily eliminated because the calculated principal directions are clearly not collinear with the experimental ones.

In this respect, model M1 performs much better: the angle deviations for all principal directions are well below the 20° mark for both the H3 and H(O2) HFC tensor. The agreement between the experimental β type HFC, HF2(F3), and the corresponding calculated tensor H3 is very good both in isotropic and in anisotropic values. Moreover, the difference in angle between the experimental and calculated principal direction for the minimum anisotropic component is remarkably good, being only 5°. The principal directions associated with the smallest and intermediate anisotropic components deviate more, but this is often observed in DFT calculations.[21] For the α-type HFC the agreement between calculated and experimental tensor is very good in terms of isotropic components and principal directions. The difference in angles for the principal direction corresponding to the minimum anisotropic component, the one that occurs when the magnetic field is parallel to the $C-H_\alpha$ bond, being only 5°. However, the anisotropy of the H3 α-type coupling (*+28*, *−4*, *−24*) is not on par with the measured data (*+15*, *0*, *−15*). In fact, similar anisotropies are found in models M2 and M4, indicating that a carbonyl group adjacent to the C_α radical center does not result in enough delocalization to reproduce the experimental anisotropy of the H_α proton coupling. The Mulliken spin densities for models M1, M2, and M4 corroborate this: the spin density is still localized for about 68% on C_α whereas the carbonyl oxygen only receives about 30%.

In model M3, the delocalization is more pronounced, since now also the pyranose ring oxygen takes part of the spin density (15%). This reduces the density on C_α to 53%, giving rise to an anisotropy for proton hyperfine tensor H6 that is more comparable to the experimental values (*+23*, *−1*, *−19*). Unfortunately, the principal directions for this hyperfine interaction are not matching their experimental counterparts. Moreover, the H4 hyperfine interaction tensor is hardly comparable to the HF2(F3) tensor.

Summarizing, the M1 model displays an overall correct pattern of HFCs and the principal directions for both the α- and β-type protons are quite close to those of the measurements. However, the anisotropy of the α-type HFC tensor is not well enough reproduced, indicating that more spin density has to be localized away from the radical center.

Radical F4/F5. As is clear from Figure 2, the hyperfine interactions of these radicals bear a remarkable similarity, suggesting that they originate from the same type of radical in two slightly different conformations. From the ENDOR angular variations two complete HFC tensors could be determined for the F4 radical, but only the biggest HFC tensor could be obtained for the F5 radical. All the determined coupling tensors (Table 2) correspond to β- or γ-type interactions.

A significant number of radicals can be formed in the fructose molecule that do not exhibit α-type interactions. One way to limit the number of possible models to consider is by examining the principal directions associated with the maximum principal values of the HF1(F4), HF2(F4), and HF1(F5) coupling tensors. For a β- or a γ-type HFC tensor, these principal directions are oriented roughly along the line connecting the center of the unpaired spin density and the interacting nucleus. Therefore, a comparison of these principal directions with the C−H directions in the pristine fructose molecule often yields a good indication of the carbon atom on which the unpaired electron is mainly localized. From the comparison in Table 4 it is clear that only when the unpaired electron is localized on C2 can a good agreement be found for all 3 HFC tensors. Only a few radical models meet the requirements that the unpaired electron is located at C2 and that α-type hyperfine interactions are not present. These models are shown in Figure 7. Model M5 is obtained after hydroxy abstraction from C2; model M6 is generated when the entire hydroxymethyl group at C2 is removed. Finally, model M7 has the unpaired electron localized at C2, with a carbonyl group at C3. In Table 5, the HFC tensors

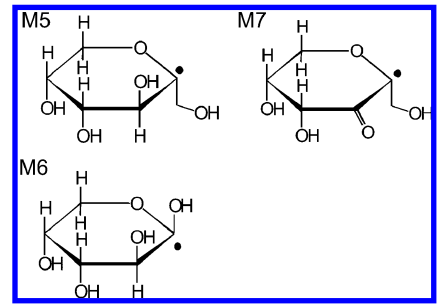

Figure 7. Chemical structure of the different models for radical F4/F5 for which DFT calculations were performed (Table 5).

TABLE 5: Proton HFC (MHz) for Radical Models M5−M7 (Figure 7), Obtained by Means of DFT Calculations

radical model	proton	isotropic values	anisotropic values	principal directions			δ (deg)[a]	
				a	*b*	*c*	F4	F5
M5	H1	9.39	−5.77	−0.810	−0.325	0.489		
			−3.33	0.365	−0.931	−0.014		
			9.09	−0.459	−0.168	−0.872		
	H1′	3.60	−5.48	0.912	0.347	0.220		
			−3.89	0.339	−0.938	0.075		
			9.44	−0.232	−0.006	0.973		
	H3	79.97	−5.32	−0.679	−0.047	−0.733		
			−1.01	−0.601	0.608	0.518		
			6.37	−0.421	−0.793	0.441		
	H6	14.70	−3.52	0.107	−0.891	0.441		
			−2.37	0.876	−0.126	−0.466		
			5.95	0.471	0.435	0.767		
M6	H3	24.49	−6.13	0.969	−0.243	0.052	31	21
			−4.33	0.047	0.383	0.923	68	65
			10.46	0.244	0.891	−0.382	59	61
	H5	9.52	−2.03	0.158	−0.985	−0.070	26	
			−1.07	0.987	0.159	−0.010	26	
			3.10	0.021	−0.068	0.997	8	
	H(O2)	10.84	−10.75	−0.835	0.147	−0.530		
			−7.77	−0.396	0.508	0.765		
			18.51	−0.382	−0.849	0.366		
M7	H1′	10.98	−3.26	−0.617	0.785	−0.054	4	
			−2.93	−0.780	−0.619	−0.096	4	
			6.21	−0.109	−0.018	0.994	1	
	H4	23.39	−2.12	1.000	−0.021	−0.009	23	16
			−1.81	−0.018	−0.966	0.260	20	13
			3.94	0.014	0.259	0.966	19	19
	H6	15.39	−2.96	0.232	−0.860	0.455		
			−1.74	0.834	−0.064	−0.547		
			4.75	0.500	0.507	0.702		

[a] δ (deg) and δ′ (deg) are the angles between the principal directions of the experimental tensors for the radicals F4 and F5 and the calculated tensors.

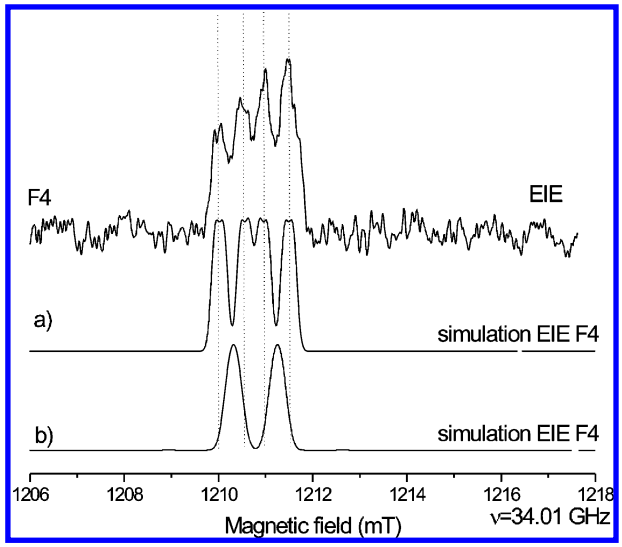

Figure 8. Simulations of the EIE spectra corresponding to the F4 radical for the magnetic field along the *a* axis for two cases: (a) when we take into account the two experimental tensors (HF1(F4) and HF2(F4)) from Table 2 and the calculated tensor H6 unassigned to any experimental tensors from Table 5 and (b) when we take into account only the two experimental tensors determined from the ENDOR angular variation.

calculated with DFT for these radical models are compared with the experimental tensors. Model M5 is not a serious candidate for the radical F4/F5 since it contains one big β-type proton hyperfine interaction (H3) that is clearly not observed in the experiment. Considering only the isotropic and anisotropic values, both models M6 and M7 could fit with the experiment. However, the principal directions of the M7 model clearly agree much better with experiment, leaving little doubt that radicals F4 and F5 have a structure that matches model M7.

The DFT calculations predict three appreciable HFCs for model M7, whereas for only two of these interactions a tensor could be determined from the ENDOR experiments. The simulation of the EIE spectrum in the *a* direction using the tensors in Table 2 (Figure 8a) clearly demonstrates that a third interaction is indeed present. Including the HFC predicted by DFT in the simulation, on the other hand, leads to very satisfactory agreement with the experimental spectrum (Figure 8b). This is an extra strong argument in favor of this radical model.

A plausible mechanism for the formation of this radical structure is shown in Figure 9. It involves a net hydrogen abstraction yielding a C3 centered radical, followed by a β elimination reaction resulting in model structure M7. The C3 carbon centered radical, which in this case is a precursor for the stable M7 radical, was previously identified as a major radical obtained after 10 or 77 K irradiation in fructose single crystals.[17,18] The fact that the precursor was observed for low temperature irradiation is also a very strong indication in favor of the M7 radical model.

TABLE 6: Comparison of the C−H Directions in the Pristine Molecule with the Directions of the Eigenvectors Corresponding to the Most Positive Anisotropic HFC Values of HF1(F6) and HF6(F6)

	hydrogen position	direction cosines			δ (deg)[a]	
		a	*b*	*c*	HF1(F6)	HF2(F6)
C2−HC1	β	0.489	0.211	0.846	35	**28**
C2−H′C1	β	−0.209	0.223	0.978	**22**	**9**
C2−HC3	β	−0.325	−0.844	0.427	33	64
C3−HC4	β	0.054	0.592	0.804	**3**	38
C4−HC3	β	0.047	0.647	0.761	**5**	42
C4−HC5	β	0.835	0.032	0.550	61	51
C5−HC4	β	0.855	−0.519	0.019	71	85
C5−HC6	β	0.313	0.853	−0.418	33	65
C5−H′C6	β	0.839	0.317	−0.443	56	59

[a] δ (deg) are the angles between the principal directions of the experimental and the calculated directions.

Radical F6. Radical species F6 exhibits two typical β-type proton HFCs: one with an isotropic HFC value of approximately 85 MHz and one around 45 MHz, in agreement with the doublet of doublets structure of the EIE spectrum observed at most orientations (see Figure 2).

To determine a likely site of the unpaired electron, again an initial comparison was made between the principal directions of the maximum principal value of the HF1(F6) and HF2(F6) coupling tensors and several C−H directions in the pristine fructose molecule. The results are shown in Table 6. A very good agreement was found between the C4−HC3 and C3−HC4 directions and the principal direction corresponding to the maximum anisotropic value of HF1(F6), suggesting that C3 or C4 could be likely sites for the unpaired electron. In addition, the C2−H′C1 direction was found to be virtually collinear with the main principal direction of HF2(F6), indicating that the unpaired electron could also be located at the C2 carbon. Since no clear indications were further available, several radical models were considered with C2, C3, or C4 as the site of the unpaired electron and DFT calculations were performed for these models (see Supporting Information). In Figure 10, an overview is presented of the models reproducing to some extent the HFC pattern observed in the measurements (one large and one intermediate β-type coupling; no α-type coupling). The corresponding calculated hyperfine tensors are given in Table 7.

Radical models M8 and M9 are obtained after a net hydrogen abstraction from C3 and C4. Model M10 could be formed after H6 abstraction and subsequent rupture of the pyranose ring, yielding a C2 centered radical species. It is not so clear how models M11−M13 would be formed. These structures were specifically pieced together in an attempt to reproduce the experimental data as closely as possible.

Reviewing only the isotropic couplings, models M8 and M11 can be eliminated since they do not have a HFC that matches

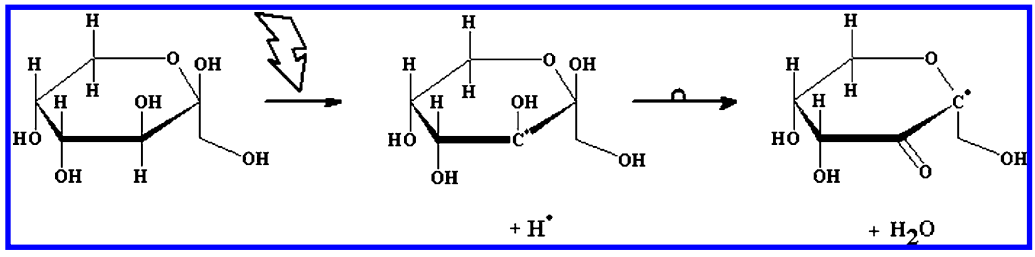

Figure 9. Plausible reaction mechanism for the formation of the M7 radical model.

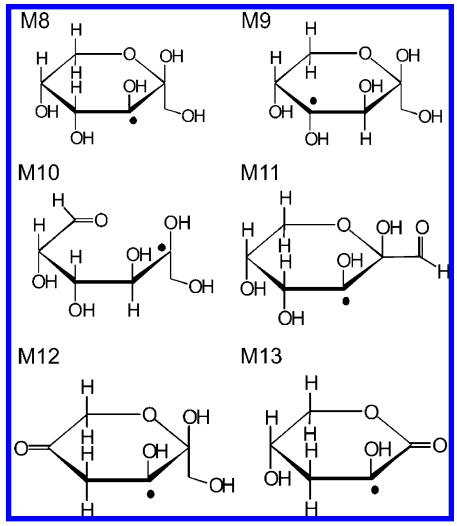

Figure 10. Chemical structures of the different models for radical F6 for which DFT calculations were performed (see Table 7).

the 45.6 MHz of HF2(F6). Model M9 does have a coupling of that size, but this is due to a hydroxy proton, yielding anisotropic values that are clearly not comparable with experimental values. Model M10 is characterized by two hyperfine interactions with the isotropic couplings in agreement with the experimental ones. The H1′ coupling tensor is matching the experimental HF2(F6) tensor very well but unfortunately this is not the case for the large β-type coupling. Analyzing the calculated principal directions, it is clear that models M12 and M13 show potential: the principal directions corresponding to the maximum anisotropic hyperfine component for the large β-type coupling deviate only 16° and 14°, respectively, with that of HF1(F6). The principal directions for HF2(F6) are also reproduced to some extent, although model M13 seems to perform much better in this respect. Considering all HFC tensors, model M13 is the most likely candidate for radical F6. Especially, the anisotropic values for the H4′ coupling are much more similar to those of HF2(F6) as compared to those for H4′ of M12.

In view of the rather good agreement between the DFT calculations and the measurements, it is tempting to conclude that M13 is a good model structure for radical F6. However, it is not entirely clear how this structure would be generated or what its precursors are. As compared to the pristine fructose structure, model M13 has to lose the H3 hydrogen, the entire hydroxymethyl group, and the H(O2) proton and the O4−H(O4) hydroxy group has to be replaced by hydrogen. Yet, these structural changes are not entirely impossible.

Conclusions

Twelve proton HFC tensors, assigned to six different radicals labeled F1−F6, could be determined from the ENDOR angular variation of RT X-irradiated fructose single crystals. Two of the radicals (F1 and F2) were previously studied by Vanhaelewyn et al.[19] and Tarpan et al.[22] In the present study the HFC tensors corresponding to the minority radicals (F3−F6) are presented, together with the proposed radical models for each of them. For the radical F3 a C3 carbon centered radical with a carbonyl group at a C4 position is proposed. For the F4/F5 radical a C2 carbon centered radical model with a carbonyl group situated at a C3 position seems appropriate. Also a C2 model is proposed for the F6 radical, but the resulting species is rather exotic and for the moment it is not clear how it can be generated.

TABLE 7: Proton HFC Tensors (MHz) for Radical Models M8−M14 (Figure 9), Obtained by Means of DFT Calculations

radical model	proton	isotropic values	anisotropic values	principal directions *a*	*b*	*c*	δ (deg)[a]
M8	H4	98.80	−5.19	−0.989	−0.094	0.116	4
			−1.72	−0.138	0.875	−0.464	8
			6.96	0.058	0.475	0.878	7
	H(O2)	18.89	−3.46	−0.753	−0.089	−0.652	88
			−1.97	−0.446	0.797	0.407	74
			5.43	−0.484	−0.597	0.640	46
	H(O3)	9.54	−10.62	−0.706	−0.556	0.438	
			−8.39	0.529	−0.826	−0.195	
			19.96	−0.471	−0.094	−0.877	
M9	H3	105.54	−5.67	−0.857	−0.355	0.374	20
			−0.81	−0.500	0.751	−0.432	19
			6.55	0.127	0.557	0.821	7
	H5	8.55	−5.34	−0.521	−0.382	0.764	
			−3.85	−0.218	0.924	0.313	
			9.19	0.825	0.003	0.565	
	H6′	7.93	−1.93	−0.041	0.817	0.576	
			−1.62	0.148	−0.565	0.812	
			3.58	0.988	0.118	−0.098	
	H(O4)	46.32	−11.75	0.251	0.685	0.684	
			−8.81	0.098	−0.721	0.686	
			20.82	−0.963	0.106	0.248	
M10	H1	100.44	−4.98	0.491	0.828	−0.270	50
			−1.43	0.835	−0.536	−0.124	58
			6.53	−0.248	−0.165	−0.955	59
	H1′	48.07	−5.27	−0.119	−0.992	−0.039	2
			−4.17	−0.893	0.124	−0.434	18
			9.39	0.435	−0.017	−0.900	18
	H(O2)	−4.82	−9.83	−0.149	0.692	0.706	
			−5.03	0.956	−0.082	0.283	
			16.11	0.253	0.717	−0.649	
	H(O3)	−4.22	−7.51	0.320	−0.904	0.283	
			0.11	−0.490	0.097	0.866	
			8.10	−0.811	−0.416	−0.412	
M11	H4	97.28	−5.23	0.988	0.080	−0.135	4
			−1.76	0.134	−0.874	0.467	8
			6.99	0.080	0.479	0.874	8
	H(O2)	19.28	−3.52	−0.748	−0.091	−0.658	89
			−2.17	−0.453	0.794	0.406	74
			5.69	−0.485	−0.601	0.635	46
	H(O3)	11.23	−11.34	−0.689	−0.585	0.429	
			−9.30	0.569	−0.802	−0.181	
			20.64	−0.450	−0.119	−0.885	
M12	H4	118.38	−4.46	−0.643	−0.732	0.225	61
			−2.74	−0.764	0.591	−0.259	62
			7.20	−0.057	0.338	0.939	16
	H4′	63.12	−5.01	−0.580	0.787	0.210	31
			−4.46	−0.812	−0.539	−0.223	26
			9.47	−0.062	−0.299	0.952	18
	H(O2)	21.16	−3.67	0.878	−0.083	0.471	
			−1.99	−0.230	0.789	0.569	
			5.66	0.419	0.608	−0.674	
	H(O3)	13.95	−10.42	−0.561	−0.741	0.369	
			−9.01	−0.684	0.666	0.297	
			19.43	−0.466	−0.086	−0.881	
M13	H4	89.36	−4.23	−0.903	−0.404	0.148	15
			−2.80	−0.430	0.842	−0.327	19
			7.03	−0.008	0.359	0.933	14
	H4′	38.25	−3.93	−0.219	0.951	0.217	14
			−2.68	0.972	0.195	0.129	3
			6.61	0.081	0.239	−0.968	14
	H(O3)	−5.92	−8.83	0.951	−0.212	−0.225	
			−7.96	−0.164	−0.963	0.213	
			16.78	0.262	0.166	0.951	

[a] δ (deg) are the angles between the principal directions of the experimental tensors for the radical F6 and the calculated tensors.

Acknowledgment. We acknowledge the Research Foundation-Flanders (Belgium) (F.W.O.-Vlaanderen) for financial support. Computational resources and services used in this work

were provided by Ghent University. We also thank Professor Einar Sagtuen, Department of Physics, University of Oslo, for the technical support regarding the orientation of the single crystals and for interest in and support of this study.

Supporting Information Available: Tables showing DFT-calculated proton HFC tensors for all the plausible radical models considered for the case of X-irradiated fructose single crystals. The radical models were obtained on the basis of typical radiation-induced reactions commonly observed in sugar systems: hydrogen abstraction/addition from/to carbon or oxygen, hydroxyl group abstraction, rupture of the sugar ring backbone, β elimination, 1,2- and 1,4-hydrogen shift, net H_2 abstraction and combinations therefore. This material is available free of charge via the Internet at http://pubs.acs.org.

References and Notes

(1) Nakajima, T.; Otsuki, T.; Hara, H.; Nishiwaki, Y.; Matsuoka, M. *Radiat. Prot. Dosim.* **1990**, *34*, 303–306.
(2) Yordanov, N. D.; Georgieva, E. *Spectrochim. Acta A* **2004**, *60*, 1307–1314.
(3) Madden, K. P.; Bernhard, W. A. *J. Phys. Chem.* **1979**, *83* (20), 2643–2649.
(4) Madden, K. P.; Bernhard, W. A. *J. Phys. Chem.* **1980**, *84* (13), 1712–1717.
(5) Vanhaelewyn, G.; Sadlo, J.; Callens, F.; Mondelaers, W.; De Frenne, D.; Matthys, P. *Appl. Radiat. Isot.* **2000**, *52*, 1221–1227.
(6) Sagstuen, E.; Lund, A.; Awadelkarim, o.; Lindgren, M.; Westerling, J. *J. Phys. Chem.* **1986**, *90* (22), 5584–5588.
(7) De Cooman, H.; Pauwels, E.; Vrielinck, H.; Dimitrova, A.; Yordanov, N.; Sagstuen, E.; Waroquier, M.; Callens, F. *Spectrochim. Acta A* **2008**, *69*, 1372–1383.
(8) De Cooman, H.; Pauwels, E.; Vrielinck, H.; Sagstuen, E.; Callens, F.; Waroquier, M. *J. Phys. Chem. B* **2008**, *112*, 7298–7307.
(9) De Cooman, H.; Pauwels, E.; Vrielinck, H.; Sagstuen, E.; Van Doorslaer, S.; Callens, F.; Waroquier, M. *Phys. Chem. Chem. Phys.* **2009**, *11*, 1105–1114.
(10) Vanhaelewyn, G.; Jansen, B.; Pauwels, E.; Sagstuen, E.; Waroquier, M.; Callens, F. *J. Phys. Chem. A* **2004**, *108*, 3308–3314.
(11) Box, H. C.; Budzinski, E. E.; Freund, H. G. *J. Chem. Phys.* **1990**, *121*, 262–266.
(12) Samskog, P. O.; Lund, A.; Nilsson, G.; Symons, M. C. R. *J. Ghem. Phys.* **1980**, *73*, 4862–4866.
(13) Samskog, P. O.; Kispert, L. D.; Lund, A. *J. Ghem. Phys.* **1983**, *79*, 635–638.
(14) Samskog, P. O.; Lund, A. *Chem. Phys. Lett.* **1980**, *75*, 525–527.
(15) Sagstuen, E.; Lindgren, M.; Lund, A. *Radiat. Res.* **1991**, *128*, 235–242.
(16) Sevilla, M. D.; Becker, D. ESR Studies of Radiation Damage to DNA and Related Biomolecules. *Electron Paramagnetic Resonance*; Series: Specialist Periodical Reports; The Royal Society of Chemistry: Cambridge, UK, 2004; Vol. 19, Chapter 6.
(17) Tarpan, M.; Sagstuen, E.; Pauwels, E.; Vrielinck, H.; Waroquier, M.; Callens, F. *J. Phys. Chem. A* **2008**, *112*, 3898–3905.
(18) Vanhaelewyn, G. C. A. M.; Pauwels, E.; Callens, F. J.; Waroquier, M.; Sagstuen, E.; Matthys, P. *J. Phys. Chem. A* **2006**, *110*, 2147–2156.
(19) Vanhaelewyn, G. C. A. M.; Lahorte, P. G. A.; De Proft, F. J. A.; Geerlings, P. F. C.; Mondelaers, W. K. P. G.; Callens, F. J. *Phys. Chem. Chem. Phys.* **2001**, *3* (9), 1729–1735.
(20) Pauwels, E.; Lahorte, P.; Vanhaelewyn, G.; Callens, F.; De Proft, F.; Geerlings, P.; Waroquier, M. *J. Phys. Chem. A* **2002**, *106*, 12340–12348.
(21) Pauwels, E.; Van Speybroeck, V.; Waroquier, M. *J. Phys. Chem. A* **2004**, *108*, 11321–11332.
(22) Tarpan, M. A.; Vrielinck, H.; De Cooman, H.; Callens, F. *J. Phys. Chem. A* **2009**, *113*, 7994–8000.
(23) Pauwels, E.; Declerck, R.; Van Speybroeck, V.; Waroquier, M. *Radiat. Res.* **2008**, *169*, 8–18.
(24) De Cooman, H.; Vanhaelewyn, G.; Pauwels, E.; Sagstuen, E.; Waroquier, M.; Callens, F. *J. Phys. Chem. B* **2008**, *112*, 15045–15053.
(25) Pauwels, E.; De Cooman, H.; Vanhaelewyn, G.; Sagstuen, E.; Callens, F.; Waroquier, M. *J. Phys. Chem. B* **2008**, *112*, 15054–15063.
(26) Pauwels, E.; De Cooman, H.; Waroquier, M.; Hole, E. O.; Sagstuen, E. *Phys. Chem. Chem. Phys.* 2010, 10.1039/C004380J.
(27) Kanters, J. A.; Roelofsen, G.; Alblas, B. P.; Meinders, I. *Acta Crystallogr. B* **1977**, *33*, 665–672.
(28) Takagi, S.; Jeffrey, G. A. *Acta Crystallogr. B* **1997**, *33*, 3510–3515.
(29) Nelson, W. H. *J. Magn. Reson.* **1980**, *38*, 71–76.
(30) Stoll, S.; Schweiger, A. *J. Magn. Reson.* **2006**, *178*, 42–55.
(31) Schonland, D. S. *Proc. Phys. Soc. London* **1959**, *73*, 788–792.
(32) Vrielinck, H.; De Cooman, H.; Tarpan, M. A.; Sagstuen, E.; Waroquier, M.; Callens, F. *J. Magn. Reson.* **2008**, *195*, 196–205.
(33) http://cp2k.berlios.de.
(34) Becke, A. D. *Phys. Rev. A* **1988**, *38*, 3098–3100.
(35) Lee, C. T.; Yang, W. T.; Parr, R. G. *Phys. Rev. B* **1988**, *37*, 785–789.
(36) Lippert, G.; Hutter, J.; Parrinello, M. *Mol. Phys.* **1997**, *92*, 477–487.
(37) VandeVondele, J.; Hutter, J. *J. Chem. Phys.* **2007**, *127*, 9–18.
(38) Goedecker, S.; Teter, M.; Hutter, J. *Phys. Rev. B* **1996**, *54*, 1703–1710.
(39) Hartwigsen, C.; Goedecker, S.; Hutter, J. *Phys. Rev. B* **1998**, *58*, 3641–3662.
(40) Declerck, R.; Pauwels, E.; Van Speybroeck, V.; Waroquier, M. *Phys. Rev. B* **2006**, *74*, 8–18.
(41) Weber, V.; Iannuzzi, M.; Giani, S.; Hutter, J.; Declerck, R.; Waroquier, M. *J. Chem. Phys.* **2009**, *131*, 11–22.
(42) Krack, M.; Parrinello, M. *Phys. Chem. Chem. Phys.* **2000**, *2*, 2105–2112.
(43) Godbout, N.; Salahub, D. R.; Andzelm, J.; Wimmer, E. *Can. J. Chem.-Rev. Can. Chim.* **1992**, *70*, 560–571.
(44) Dizdaroglu, M.; Leitich, J.; Von Sonntag, C. *Carbohydr. Res.* **1976**, *47*, 15–23.
(45) Abagyan, G. V.; Apresyan, A. S. *High Energy Chem.* **2004**, *38*, 369–372.
(46) McConnell, H. M. *J. Chem. Phys.* **1956**, *24*, 764–766.
(47) Heller, C.; McConnell, H. M. *J. Chem. Phys.* **1960**, *32*, 1535–1540.
(48) Erling, P. A.; Nelson, W. H. *J. Phys. Chem.* **2004**, *108*, 7591–7595.
(49) Bernhard, W. A. *Adv. Radiat. Biol.* **1981**, *9*, 199–280.
(50) Bernhard, W. A. *J. Chem. Phys.* **1984**, *81*, 5928–5936.

JP107777V